Biosensors and Bioelectronics 26 (2010) 1131–1136

Contents lists available at ScienceDirect

Biosensors and Bioelectronics

journal homepage: www.elsevier.com/locate/bios

Nanoplasmonic biosensing with on-chip electrical detection☆

Francesco Mazzotta, Guoliang Wang, Carl Hägglund, Fredrik Höök*, Magnus P. Jonsson**

Department of Applied Physics, Chalmers University of Technology, SE-41296 Gothenburg, Sweden

ARTICLE INFO

Article history:
Received 13 April 2010
Received in revised form 2 July 2010
Accepted 2 July 2010
Available online 31 July 2010

Keywords:
Localized surface plasmon resonance
Biosensor
Bioanalytical sensing
Nanodisks
Photo diode
Solar cell

ABSTRACT

A nanoplasmonic biosensor chip with integrated electrical detection is presented. The concept is based on the local refractive index sensitivity of nanoplasmonic gold nanodisks (110 nm in diameter and 20 nm in height) that are fabricated, through a parallel method, directly on an array of silicon solar cells or photoactive diodes. The nanoplasmonic properties of the sensor chip were investigated both optically and electrically, with excellent agreement between the two. We show that local changes in the refractive index of the surrounding environment gives changes in the nanoplasmonic properties of the gold nanodisks, which induce corresponding changes in the photocurrent at single wavelengths of the nanoplasmonic solar cells. With a simple light-emitting diode as light source, and together with a material-specific modification protocol, the photocurrent output of the nanoplasmonic sensor chip was successfully used to monitor a specific biorecognition reaction in real-time.

1. Introduction

The development of small, cheap and robust bioanalytical sensors is important, for example, with respect to medical diagnostics and in particular for use at point-of-care. Preferably, the sensor method should not require neither pre- nor post-modification with fluorophores or other labels. Instead, the presence of a target molecule should be measured directly through changes in the electrical (Grieshaber et al., 2008), mechanical (Janshoff et al., 2000) or optical (Liedberg et al., 1983) properties of the sensor device. Apart from such *label-free* sensing, it is valuable to be able to measure in *real-time*, as this will provide both a rapid detection and kinetic information on the interactions under investigation.

With respect to label-free and real-time bioanalytical sensing, metal nanostructures have shown great promise (Jonsson et al., 2008a; Stewart et al., 2008). Noble metal nanostructures scatter and absorb light efficiently at certain wavelengths, because photons can be converted into localized surface plasmons. These nanoplasmons are coherent oscillations of the conduction electrons in the metal and they are excited at specific resonance wavelengths. For gold and silver nanoparticles, the resonances typically lie within the visible wavelength range. This gives the particles distinct colours, which for instance have been used to stain glass for centuries. The localized surface plasmon resonance (LSPR) is highly dependent on the refractive index (RI) of the local environment surrounding the particles, which can be utilized for label-free and real-time bioanalytical sensing (Englebienne, 1998). This is based on the fact that target molecules binding to receptors on the surface of a nanoplasmonic structure will induce changes in the local RI. The reaction may therefore be followed through the nanoplasmonic resonance by, for example, monitoring of the temporal variation in the wavelength at maximum extinction (peak position).

Nanoplasmonic sensors have the potential to be used for rapid, simple and low-cost medical diagnostics. Apart from being competitive with respect to sensor performance (Svedendahl et al., 2009), one main reason for this expectation is simplicity. For example, in contrast to conventional surface plasmon resonance (SPR) sensors based on flat metal films (Liedberg et al., 1983), nanoplasmonic sensors do not require a prism to couple light to plasmons. Instead, the LSPR can be excited without any restrictions on the angle of incidence, including at normal incidence. Apart from making the instrumentation less complicated, this also facilitates the direct combination of nanoplasmonic sensing with sensor techniques that rely on other physical transduction principles (Dahlin et al., 2008; Jonsson et al., 2008b). Furthermore, the sensitivity is highly confined to the surface of nanoplasmonic sensors. In fact, the field decay length of LSPR sensors is around one order of magnitude shorter compared with that of SPR sensors (Jonsson et al., 2008a). This means that LSPR sensors are less sensitive to variations in the bulk medium outside the region of interest and that, for example, temperature control is typically not needed. While the short decay length of nanoplasmonic sensors can also be uti-

☆ Winner of the 2010 Biosensors and Bioelectronics Award for the most original contribution to the Congress.

* Corresponding author. Tel.: +46317726130; fax: +46317723134.
** Corresponding author. Tel.: +46317725172; fax: +46317723134.
E-mail addresses: fredrik.hook@chalmers.se (F. Höök), magnus.p.jonsson@chalmers.se (M.P. Jonsson).

0956-5663/$ – see front matter © 2010 Elsevier B.V. All rights reserved.
doi:10.1016/j.bios.2010.07.008

lized for other purposes, such as to study biomolecular structural changes (Hall et al., 2008; Jonsson et al., 2007, 2008b), a longer plasmonic field penetration depth, as that for conventional SPR sensors, may be preferable for certain applications where many and/or very thick biomolecular layers are used. It should be noted that the simplicity of LSPR sensors also includes their fabrication. This is owed to recent development of cheap and scalable methods that allow for highly controllable and reproducible fabrication of plasmonic structures on large (>1 cm^2) areas (Fredriksson et al., 2007; Hanarp et al., 2003; Hendren et al., 2008; Henzie et al., 2007; Hulteen and van Duyne, 1995; Malyarchuk et al., 2005; Nagpal et al., 2009).

A typical nanoplasmonic sensor setup is based on a white light source, a flow cell with the sensing structure and a photospectrometer, where mainly the latter is rather bulky and costly and limits the use of nanoplasmonic sensing for, for example, point-of-care diagnostics. However, as shown in the very first nanoplasmonic biosensor report by Englebienne (1998), it is possible to monitor plasmon shifts through the change in light extinction at a single wavelength. This is promising with respect to reduced size and cost of the experimental setup considering that there are small and low-cost high-intensity light-emitting diodes (LED) available on the market. Further, instead of a spectrometer, one or several photosensitive diodes can be used as detectors. For example, Neuzil and Reboud (2008) used four-pulsed powered LEDs, a photodiode and a lock-in amplifier to develop a small LSPR sensor device.

With the aim to simplify the LSPR sensor concept even further, we here present a nanoplasmonic biosensor with integrated electrical detection. As schematically depicted in Fig. 1a, the sensor is based on a chip with an array of four small (2 mm × 0.14 mm) photoactive diode regions. These regions are silicon p/n junctions and act as four independent photo detectors. On two of these diodes, a short-range ordered array of nanoplasmonic gold nanodisks were made by hole-mask colloidal lithography, a parallel nanofabrication method based on the self-assembly of nanocolloids (Fredriksson et al., 2007). The shift in the plasmon resonance of the gold nanodisks, as induced by a biomolecular binding reaction, will give a shift in the extinction (and transmission) at a wavelength where the slope of the LSPR peak is high (Fig. 1b). This modulates the light intensity in the photoactive regions of the patterned diodes, and thereby induces changes in their photocurrent outputs (Fig. 1c). The two unpatterned diodes are used as references to account for potential variations in the light source and other experimental parameters. With the aim to minimize the cost and size of the setup, a small high-intensity LED was used as light source. After optimization of the dimensions of the nanoplasmonic structure with respect to the optical properties and the corresponding sensitivity to RI changes, nanoplasmonic diode sensor chips were characterized both optically and electrically. Finally, the on-chip electrical detection concept was used to monitor a specific biorecognition reaction in real-time.

2. Materials and methods

2.1. Materials

Unless otherwise stated, materials and chemicals were purchased from Sigma–Aldrich AB, Sweden.

2.2. Fabrication of nanoplasmonic diode sensor chips

The sensor chips were made from 380-μm thick n-doped silicon wafers (Si (1 0 0), Si-Mat, Germany). Ion implantation was used to define arrays of four p-doped regions, each 2 mm× 0.14 mm in size. These will be the photosensitive diode regions in the final device. Thin aluminium (Al) electrodes were fabricated by conventional photolithography (MA/BA6, SUSS MicroTec, Germany) and sputter deposition (MS150, FHR Anlagenbau GmbH, Germany) along the diode areas. These electrodes were designed to end as larger contact pads around 5 mm away from the p/n junctions. The whole wafer (except from on the contact pads) was coated with a thin layer of 30 nm silicon dioxide (SiO_2) and 60 nm silicon nitride (SiN) by plasma enhanced chemical vapour deposition (PECVD, Surface Technology Systems, Newport, UK) for electrical insulation. Titanium and gold (Ti/Au) were sputter deposited on the backside of the wafer to act as backside electrode. The wafer was then cut into smaller sensor chips, each with four separate photodiodes.

Nanoplasmonic gold nanodisks were fabricated on two of the four diodes using hole-mask colloidal lithography, as described in detail by Fredriksson et al. (2007). In brief, a thin layer of poly(methyl methacrylate) (PMMA) was spin coated onto a sensor chip. After oxygen plasma treatment to reduce the hydrophobicity of the PMMA, the surface was functionalized with an electrolyte (Aluminum Chlorohydrate, Reheis, US). Next, 110 nm in diameter polystyrene nanoparticles (Interfacial Dynamics corporation, US) were allowed to adsorb in a self-assembled short-range order on the surface. The colloids were then removed by tape stripping from all areas, except from on two of the four diodes. Next, a chromium (Cr) etch mask was created by e-beam assisted evaporation (AVAC HVC600, Applied Vacuum Scandinavia AB, Sweden) and subsequent tape stripping of the rest of the colloids. The holes in the Cr mask on the two diodes were transferred into the PMMA by oxygen plasma (Batch Top RIE, Plasma Therm, US). Finally, short-range ordered gold nanodisks were created on the diodes by e-beam assisted evaporation of 1 nm Cr and 20 nm gold (Au) and subsequent PMMA lift off. The Cr was used to enhance the adhesion between the Au disks and the SiN layer in order to improve the quality and reusability of the sensors chips.

2.3. Fabrication of test structures

Test structures were fabricated on SiN-coated (same type of SiN as for the sensor chips) 1-in. glass slides (0.2 mm in thickness, Menzel-Gläser, Germany) according to the protocol described above, but using varying diameter of the polystyrene colloids and varying Au thickness.

2.4. Characterization of test structures

Extinction spectra of gold nanodisks on the SiN-coated glass samples were acquired using a transmission-based LSPR sensor setup based on a white light source (tungsten–halogen lamp, HL-2000, Ocean Optics, US) and a photodiode array spectrometer (BRC711E, B&WTek, US). The extinction (absorption + scattering) is measured in absorbance units (Abs) and defined as $extinction = -\log_{10}(intensity_{sample}/intensity_{reference})$. The corresponding percentage of light that is transmitted through the sample can then be directly obtained as $transmission = 100 \times 10^{-extinction}$ ($transmission = 100 \times intensity_{sample}/intensity_{reference}$). The transmission-based setup was also used to investigate the influence from small changes in RI on the optical properties of the test structures by immersion in different glycerol concentrations of known refractive indices (Hoyt, 1934).

2.5. Characterization of the nanoplasmonic sensor chip

Because the Si-based sensor chip is not transparent, the optical properties of the final sensor could not be probed in transmission-mode. Instead they were investigated in reflection-mode using a conventional microscope equipped with a spectrometer (QE65000, Ocean Optics, US). The reflected light from both an unpatterned diode without gold nanodisks (R_{ref}) and one with gold nanodisks

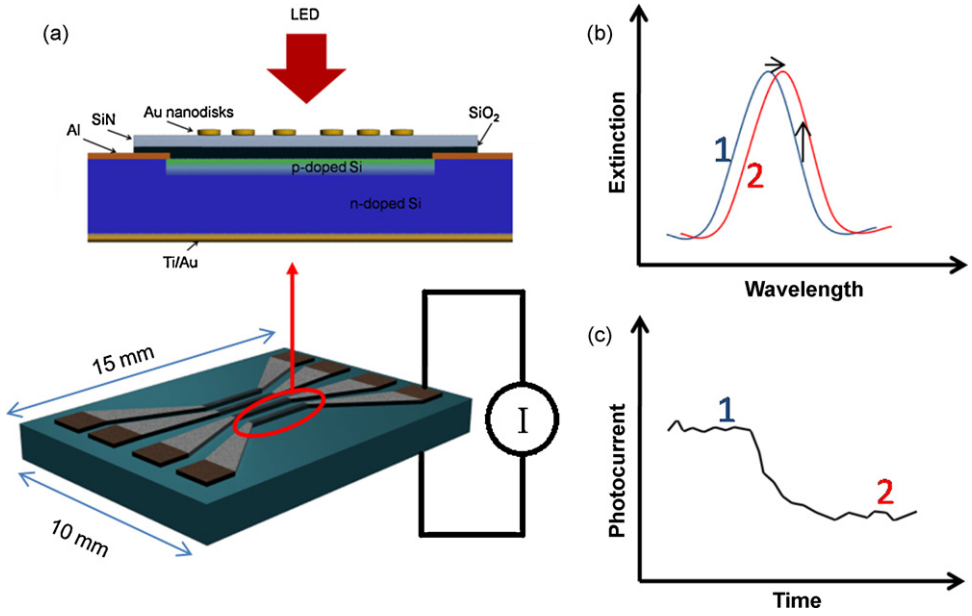

Fig. 1. Illustration of the sensor device and the sensing principle. (a) The bottom image shows a schematic illustration of the sensor chip with four photoactive diodes (2 mm × 0.14 mm) of which two are references and two (circled) are patterned with gold nanodisks. The top image shows a cross-section of one of the diodes with gold nanodisks. (b) The graph illustrates how a redshift (1–2) of the extinction peak results in both a change in peak position and a change in the extinction at a given wavelength. (c) This graph illustrates how the change in extinction (1–2) and corresponding change in light reaching the nanoplasmonic diodes, is expected to be converted into a change in the photocurrent of the sensor device that can be measured in real-time. The schematics are not to scale.

($R_{plasmon}$) were measured and the influence of the disks was evaluated as the *reflection ratio* = $R_{plasmon}/R_{ref}$.

The spectral photovoltaic response of the sensor chip was measured using a potentiostat (FAS1, Gamry, US), a white light source and a set of bandpass filters (400–900, 10 nm full-width at half-maximum) (Hägglund et al., 2008b). The photocurrent of a nanoplasmonic diode ($I_{plasmon}$) and a reference diode (I_{ref}) was measured and the influence from the gold nanodisks was evaluated as the *photocurrent ratio* = $I_{plasmon}/I_{ref}$, at each filter wavelength.

2.6. Functionalization of the sensor chip

The surface of the chip was modified to promote subsequent selective and specific binding of NeutrAvidin on the Au disks only. First, a drop containing a 0.3 mg/mL 4:1 (by weight) mixture of 3 kDa thiol-modified poly(ethylene glycol) (thiolPEG) and 5 kDa biotinylated thiolPEG (thiolPEGbiotin) (Rapp Polymere GmbH, Germany) dissolved in 10 mM Hepes buffer (4-(2-hydroxyethyl)-1-piperazineethanesulfonic acid) with 150 mM NaCl at pH 7.4, was placed on the diodes and allowed to bind on the Au disks for 2 h. After rinsing thoroughly with MilliQ water (Millipore, US) and blow drying with nitrogen, a drop of the same buffer containing 0.01 mg/mL PEG grafted to poly-L-lysine (PLL-*g*-PEG, SuSoS AG, Switzerland) was instead placed on the sample and allowed to bind to the SiN. As addressed below and previously shown (Jonsson et al., 2010), PLL-*g*-PEG binds only to the SiN and not to the functionalized gold surface. After 1 h incubation, the sensor device was again rinsed thoroughly with MilliQ water and blow-dried.

2.7. Biosensing with the nanoplasmonic sensor chip

For photocurrent ratio sensitivity measurements and biosensing experiments, the sensor chip was mounted in a custom-made titanium flow cell allowing for liquids to be flown over the diodes using a peristaltic pump (Ismatec, Switzerland). The contact pads were located outside the flow cell and one plasmonic and one reference diode were connected to a homemade electronic board functioning as a current–voltage converter. Note that even though a current–voltage converter was used and the output was given in volts (V), the output is still denoted "photocurrent" and "photocurrent ratio" to avoid confusion. This board was connected to a data-acquisition pad (LabJack Corporation, US) and the signals were finally recorded and plotted using a custom-designed LabVIEW program (National Instruments, US). The flow cell had a glass lid to allow light from a high-intensity, narrow-angle LED at 780 nm (LED780E, Thorlabs, UK) to reach the diodes. The measurements were performed without any temperature control.

3. Results and discussion

3.1. Optimization of the nanoplasmonic structure

The main aim with the nanoplasmonic test structures was to establish the optimal gold nanodisk dimensions to be used on the photodiode sensor chips. To mimic the final sensor chip design, the test structures were fabricated on SiN-coated glass slides instead of directly on glass. The extinction spectra in air for 20 and 40 nm high gold nanodisks with diameters 51, 80 and 110 nm (six different structures) are shown in Fig. 2a. Overall, the maximum extinction increased with diameter, while it was influenced less by the height of the disks. As expected from previous reports on plasmonic gold nanodisks (Hanarp et al., 2003), the peak position redshifted with increasing aspect ratio. That is, the peak redshifted with increasing diameter and blueshifted with increasing height of the disks. This makes it possible to tune the peak throughout the visible wavelength range. The use of nanoplasmonic structures for sensing stems from the sensitivity of the optical properties to changes in RI of the local environment. This was investigated for the test structures by immersing them in different concentrations of glycerol with known refractive indices. As exemplified for 110 nm in diameter and 20 nm high disks (red curve in Fig. 2b), the position of the LSPR peak shifted linearly with changes in RI. The *peak position sensitivity* (defined as peak shift versus change in bulk RI) of

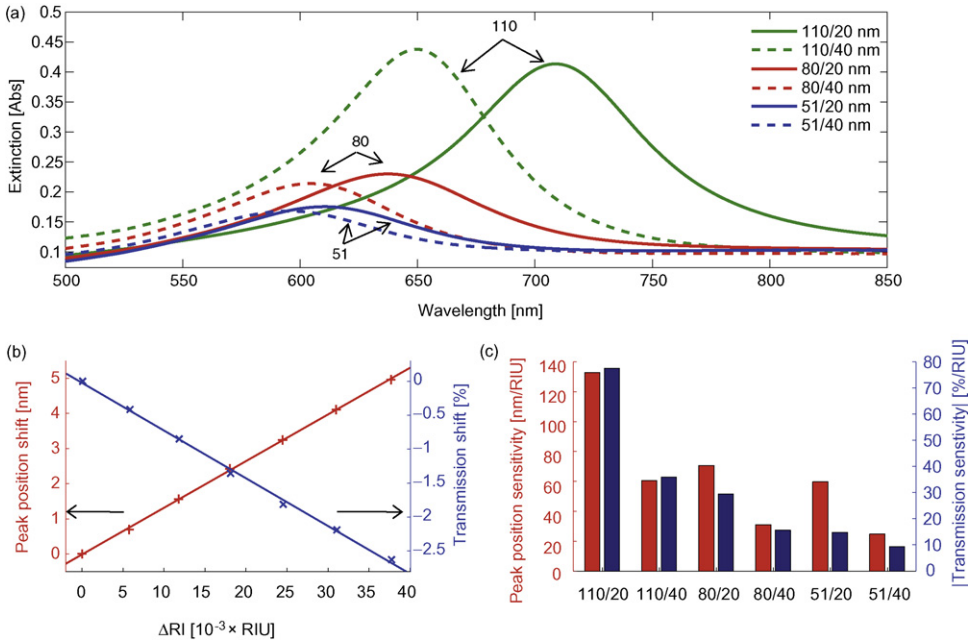

Fig. 2. Characterization of the test structures. (a) Extinction spectra in air. The disk dimensions are shown as diameter/height in the legend. The variation in peak position for disks with the same geometry was less then 1% (relative standard deviation) as measured for five different samples (from three different batches) with 110 nm in diameter and 20 nm high disks (data not shown). (b) The graph shows the change in both peak position (red) and transmission (blue, at 772 nm) versus the change in RI for 110 in diameter and 20 nm high disks on SiN-coated glass slides. The full lines are linear fits to the experimental data. (c) The bar plot shows the sensitivity in peak position (red, left bars) and transmission (absolute values, blue, right bars) to changes in RI for all structures investigated. The dimensions are shown as diameter/height in nanometers. (For interpretation of the references to color in this figure legend, the reader is referred to the web version of this article.)

each plasmonic structure could then be calculated as the slope of linear fits to the experimental data. The corresponding sensitivities for all structures are displayed as the red bars in Fig. 2c. It is clear that the 110 nm in diameter and 20 nm high gold disks had the highest peak position sensitivity with a value of around 133 nm RIU^{-1} (RIU = refractive index units). This was also the structure with the peak position at the longest wavelength (full green line in Fig. 2a), in agreement with previous reports (Hanarp et al., 2003; Miller and Lazarides, 2005). Although disks at peak positions at even longer wavelengths are expected to provide higher sensitivity (Miller and Lazarides, 2005), we choose to stick to these six different geometries in this study, primarily to stay within the wavelength range of our setups. Note that the nanoplasmonic sensor chip will not measure changes in peak position, but the signal will be directly related to the absolute change in the intensity of light that reaches the plasmonic diode at the wavelength of the LED. The blue curve in Fig. 2b shows the change in light transmission versus change in RI at 772 nm (the wavelength corresponding to the highest slope to the right of the peak) for the 110 nm in diameter and 20 nm high gold disks. It is clear that there is also in this case a linear relation. The slope of the linear fits to these types of curves could then be used to calculate the *transmission sensitivity* (defined as the change in transmission versus change in bulk RI) for each structure. This was done at the highest slope on both sides of the peak (in water) and the largest absolute values for all structures are presented as the blue bars in Fig. 2c. Interestingly, the peak position sensitivity and transmission sensitivity do not correlate perfectly. For example, the 110 nm in diameter and 40 nm high disks have a lower peak position sensitivity compared with the 80 nm in diameter and 20 nm high disks, but significantly higher transmission sensitivity. This is due to the fact that the transmission sensitivity is not only related to shifts in the peak position, but it is also dependent on the peak width and the height of the peak (absolute extinction). It can be concluded that the 110 nm in diameter and 20 nm high disks are superior also with respect to transmission sensitivity and this geometry was therefore chosen for the photodiode sensor chips.

3.2. Optical and electrical characterization of the nanoplasmonic sensor chips

Sensor chips with 110 nm in diameter and 20 nm high short-range ordered gold nanodisks were fabricated as described above. The ratio between the reflected light from a diode with nanodisks and a reference diode region without nanodisks is shown as the red trace in Fig. 3a. A clear increase is observed in the reflection ratio at around 730 nm. This wavelength is in reasonable agreement with the extinction peak position at 710 nm in air for the corresponding test structure. The around 30% increase in collected light at the plasmon resonance for the nanopatterned region compared with the non-patterned region is attributed mainly to light backscattered by the nanodisks. This is supported by around 30% light being backscattered at the plasmon resonance for the corresponding test structure, as measured using an integrating sphere (data not shown).

For the nanoplasmonic diodes to function as biosensors with direct electrical read-out, it is essential that the plasmonic properties can be probed electrically. This was evaluated as the ratio (at different wavelengths) between the photocurrents of one of the two plasmonic diodes and one of the reference diodes. As shown in Fig. 3a (blue markers), there is a clear dip in the photocurrent ratio around the plasmonic resonance, with a minimum between 720 and 760 nm, close to 740 nm. This in is perfect agreement with the peak position in the reflection ratio for the same sensor chip. The dip is attributed to less light reaching the diode patterned with gold nanodisks due to absorption and back scattering (Hägglund et al., 2008b). Note that the minimum value of around 0.4 in the current ratio is in agreement with around 40% light transmission at the plasmon resonance, as observed for the corresponding test structure (see green full line

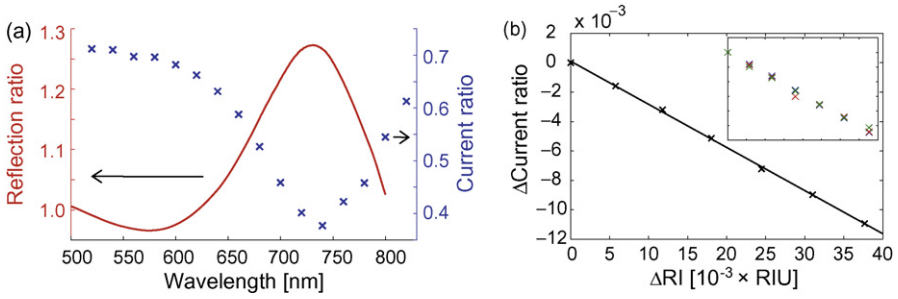

Fig. 3. Characterization of sensor chips with 110 nm in diameter and 20 nm high disks. (a) The red curve shows the optical reflection ratio ($R_{plasmon}/R_{ref}$) in air and the blue markers show the photocurrent ratio versus optical wavelength in air. (b) Change in current ratio at 780 nm versus change in RI for a sensor chip. The full line is a linear fit to the experimental values and the slope represents the photocurrent ratio sensitivity. The inset shows the experimental values for measurements on three different nanoplasmonic sensor chips as a means to illustrate the reproducibility of the method (the scales and labels are the same as for the larger graph). The standard deviation of the current ratio sensitivity was 0.01 RIU^{-1}. This corresponds to a variation of around 3.5%. A small drift in the signal was corrected for in one of the measurements. (For interpretation of the references to color in this figure legend, the reader is referred to the web version of this article.)

in Fig. 2a, 0.4 in extinction corresponds to 40% light transmission).

Because the plasmonic properties were observed in the electrical properties of the sensor chip, a change in RI is expected to result in a change in the photocurrent ratio at a given wavelength (similar to the transmission sensitivity measured for the test structures). In this respect it is important to choose a light source at an appropriate emission wavelength. For the test structure with 110 nm in diameter and 20 nm high disks, the transmission sensitivity was 78%/RIU to the left (at 712 nm) and −70%/RIU to the right (at 772 nm) of the peak. The different signs can be explained from the fact that a red shift of the plasmon peak gives an increase and decrease in transmission to the left and to the right of the peak, respectively. Because the values are comparable and a high-intensity LED with emission at 780 nm was commercially available, such an LED was chosen to probe changes in the photocurrents and the current ratio. Similarly to the optimization of the test structures, the sensitivity of the nanoplasmonic sensor chips was investigated by immersion in different concentrations of glycerol. From Fig. 3b it is seen that the current ratio decreases linearly with changes in RI. The *photocurrent ratio sensitivity*, defined as the change in photocurrent ratio versus change in bulk RI, was determined to be −0.29 RIU^{-1}. The reproducibility of the method was investigated by performing bulk sensitivity measurements for three different sensor chips (see inset in Fig. 3b). The variation in sensitivity in terms of standard deviation was determined to be less than 0.01 RIU^{-1}, corresponding to a relative standard deviation of around 3.5%. Note that the sign of the photocurrent ratio sensitivity is in agreement with the negative value of the transmission sensitivity obtained to the right of the peak for the test structure. If the photocurrent is assumed to be directly proportional to the intensity of light that reaches the diodes, the photocurrent ratio × 100 should give a rough estimate on the transmission (compare the definition of photocurrent ratio and the definition of transmission above). The values of the sensitivities for the sensor chip and corresponding test structure can then be compared directly, yielding −29%/RIU and −70%/RIU, respectively. The difference of more than a factor 2 will be investigated in future work and is tentatively attributed to small differences in the plasmonic properties of the sensor chip and the test structure. The difference may also be a result from differences between the experimental setups, such as the fact that the reference was acquired before each measurement for the test structures, while it was acquired continuously using the built-in reference for the sensor chips. The important point, however, is that changes in the nanoplasmonic properties, induced by changes in the bulk RI, could be directly measured electrically using these sensor chips. Below, we investigate if also *local* changes in RI can be measured with a sufficient signal-to-noise ratio to probe biomolecular binding reactions.

3.3. Electrical detection of specific protein binding

Finally, the sensor chips were evaluated with respect to real-time investigation of a specific biomolecular binding reaction. In this respect it is important not only to control the surface chemistry of the gold disks, but also of the surrounding SiN. The reason is mainly that unspecific adsorption to SiN regions close to the gold disks may induce false shifts in the plasmon resonance. Also, both the binding rate and the limit of detection of nanosensors can be improved by restricting molecules to bind to areas with high sensitivity only (i.e. the gold disks in this case) (Feuz et al., 2010). This motivates the use of material-specific surface modifications, where PEG-based (poly(ethylene glycol)) chemistry has previously shown successful for Au and SiN (Jonsson et al., 2010). PEG is known to pre-

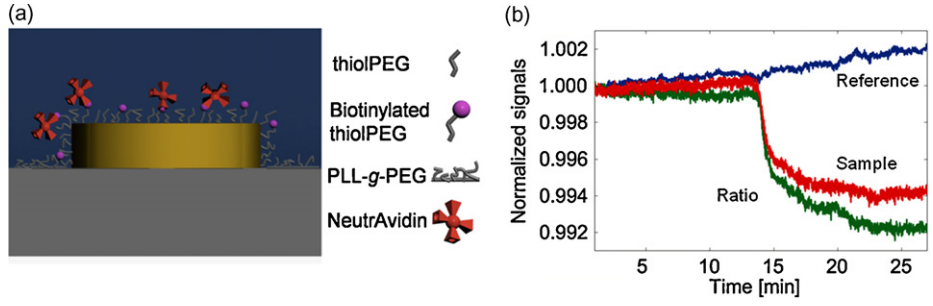

Fig. 4. Biosensing with the nanoplasmonic sensor chip. (a) Schematic illustration of the surface chemistry enabling NeutrAvidin to bind specifically on gold, while adsorption is prevented on SiN. (b) The three curves show the normalized photocurrents of the plasmonic diode (red) a reference diode (blue) and the photocurrent ratio (green) during the binding of NeutrAvidin to the gold nanodisks. The NeutrAvidin was added at around 13 min and the flow cell was rinsed with buffer again at around 22 min. The curves were normalized with the corresponding starting values of 1.679 V (blue), 0.693 V (red) and 0.413 (green). (For interpretation of the references to color in this figure legend, the reader is referred to the web version of this article.)

vent unspecific binding of biomolecules in general (Kenausis et al., 2000) and by having one end modified with a thiol (thiolPEG) it will bind preferentially to Au, while it will not adsorb on SiN. Furthermore, by having a fraction of the thiolPEG modified with a bioactive group (biotin in this study) it is possible to activate the Au disks for subsequent biomolecular binding (NeutrAvidin in this study). After functionalizing the gold disks, the surrounding SiN was passivated with PEG grafted to poly-L-lysine (PLL-*g*-PEG). PLL-*g*-PEG binds to SiN, but not to the functionalized Au surface (Jonsson et al., 2010). The resulting structure promotes specific binding of NeutrAvidin on the Au disks, while unspecific adsorption on SiN is prevented, as depicted schematically in Fig. 4a (see Section 2 for detailed information on the surface modification scheme). The sensor chip was then mounted in the measurement setup and exposed to 10 mM Hepes buffer followed by a solution of 100 μg/mL NeutrAvidin dissolved in 10 mM Hepes buffer. The resulting sensor signals were normalized and plotted in the same graph for comparison (Fig. 4b). The NeutrAvidin was added at around 13 min. In agreement with the expectations, the photocurrent of the plasmonic diode (red) decreases upon NeutrAvidin binding. In contrast, the signal from the reference diode (blue) was not influenced by the addition of NeutrAvidin. Note, in particular, that there was no detectable shift in the reference signal even when the SiN was not passivated with PLL-*g*-PEG, i.e. under conditions promoting NeutrAvidin binding to SiN (data not shown). This is a strong indication that the shift observed in the plasmonic response upon NeutrAvidin binding is due to the redshift of the plasmonic peak and the corresponding decrease in light intensity that reaches the diode p/n junction. Note that there is a small, but clear drift in both the plasmonic and the reference response. This could be due to drift in the intensity of the LED or other experimental parameters. This drift is not seen in the ratio between the two signals (green), illustrating the benefit of having a built-in reference that can be used to distinguish the nanoplasmonic response from other effects. The signal-to-noise ratio was approximately 20 (at an acquisition rate of around 0.8 Hz) for the photocurrent ratio response, slightly better than when using the nanoplasmonic signal only. For the present sensor design, buffers with a salt concentration lower than that corresponding to physiological conditions were used in the real-time measurements. The reason was that drifts and/or spikes were observed when buffers with additional salt were used, which could be a result from the conductivity of such buffers influencing the diodes via cracks or other defects in the SiO_2/SiN coating. This will be improved in the next generation of the sensor design, for example, using a spacer layer between the nanoplasmonic structure and the diodes.

4. Concluding remarks

In conclusion, a nanoplasmonic biosensor with integrated electrical read-out was developed. With simple means, it was shown capable of recording the selective and specific binding of protein to receptors immobilized on gold nanodisks placed directly on a photoactive diode. Moreover, a built-in reference signal was shown to improve both the stability and the signal-to-noise ratio of the sensor. While more complicated and expensive LSPR sensor setups may still provide a better signal-to-noise ratio, we believe the simplicity of the presented system is essential and that the concept has a potential for the development of, for example, hand-held devices and point-of-care medical instruments. We also anticipate that the performance of the concept may benefit from the use of multiple LEDs or other light sources, together with photodiodes that are sensitive at different regions of wavelengths (for example, a colour-CCD [charged coupled device]). Further, the use of commercially available high-density photodiode arrays also points towards the potential for extending the concept to high-throughput multiplex sensing. The possibility for miniaturization is further supported by the fact that signals even from single plasmonic particles can be detected electrically, as demonstrated by De Vlaminck et al. (2007). As mentioned above, the next generation of nanoplasmonic sensors with on-chip detection may benefit from having a spacer layer between the photo diodes and the sensing structures. In this way, the nanoplasmonic structure could potentially be a consumable, while the photodiodes could be reused. However, it may also be interesting to investigate near-field effects by instead having the nanoplasmonic structure in direct contact with a semiconductor layer, as was previously investigated both theoretically and experimentally with respect to plasmon-enhanced photovoltaic efficiency (Hägglund and Kasemo, 2009; Hägglund et al., 2008a,b). Finally, aiming for a portable and cheap LSPR sensor device, the potential of integrating not only the detector, but also the light source directly on the chip would be a natural extension of this work (Hedsten et al., 2010).

Acknowledgement

The authors thank Laurent Feuz for discussions on the surface modification. The work was financially supported by a scholarship from St. Jude Medical and the INGVAR grant from the Swedish Foundation for Strategic Research.

References

Dahlin, A.B., Jonsson, P., Jonsson, M.P., Schmid, E., Hook, F., 2008. ACS Nano 2 (10), 2174–2182.
De Vlaminck, I., Van Dorpe, P., Lagae, L., Borghs, G., 2007. Nano Lett. 7 (3), 703–706.
Englebienne, P., 1998. Analyst 123 (7), 1599–1603.
Feuz, L., Jönsson, P., Jonsson, M.P., Höök, F., 2010. Acs Nano 4 (4), 2167–2177.
Fredriksson, H., Alaverdyan, Y., Dmitriev, A., Langhammer, C., Sutherland, D.S., Zaech, M., Kasemo, B., 2007. Adv. Mat. 19 (23), 4297–4302.
Grieshaber, D., MacKenzie, R., Vörös, J., Reimhult, E., 2008. Sensors 8 (3), 1400–1458.
Hägglund, C., Kasemo, B., 2009. Opt. Expr. 17 (14), 11944–11957.
Hägglund, C., Zäch, M., Kasemo, B., 2008a. Appl. Phys. Lett. 92 (1), 013113–113113.
Hägglund, C., Zäch, M., Petersson, G., Kasemo, B., 2008b. Appl. Phys. Lett. 92 (5).
Hall, W.P., Anker, J.N., Lin, Y., Modica, J., Mrksich, M., Van Duyne, R.P., 2008. J. Am. Chem. Soc. 130 (18), 5836–5837.
Hanarp, P., Kall, M., Sutherland, D.S., 2003. J. Phys. Chem. B 107 (24), 5768–5772.
Hedsten, K., Fonollosa, J., Enoksson, P., Modh, P., Bengtsson, J., Sutherland, D.S., Dmitriev, A., 2010. Anal. Chem. 82 (4), 1535–1539.
Hendren, W.R., Murphy, A., Evans, P., O'Connor, D., Wurtz, G.A., Zayats, A.V., Atkinson, R., Pollard, R.J., 2008. J. Phys. Condens. Matter. 20 (36).
Henzie, J., Lee, M.H., Odom, T.W., 2007. Nat. Nanotechnol. 2 (9), 549–554.
Hoyt, L.F., 1934. Ind. Eng. Chem. 26 (3), 329–332.
Hulteen, J.C., van Duyne, R.P., 1995. J. Vacuum Sci. Technol. A – Vacuum Surf. Films 13 (3), 1553–1558.
Janshoff, A., Galla, H.J., Steinem, C., 2000. Angew. Chem. Int. Ed. 39 (22), 4004–4032.
Jonsson, M.P., Dahlin, A.B., Feuz, L., Petronis, S., Hook, F., 2010. Anal. Chem. 82 (5), 2087–2094.
Jonsson, M.P., Dahlin, A.B., Jönsson, P., Höök, F., 2008a. Biointerphases 3 (3), FD30–FD40.
Jonsson, M.P., Jönsson, P., Dahlin, A.B., Höök, F., 2007. Nano Lett. 7 (11), 3462–3468.
Jonsson, M.P., Jönsson, P., Höök, F., 2008b. Anal. Chem. 80 (21), 7988–7995.
Kenausis, G.L., Voros, J., Elbert, D.L., Huang, N.P., Hofer, R., Ruiz-Taylor, L., Textor, M., Hubbell, J.A., Spencer, N.D., 2000. J. Phys. Chem. B 104 (14), 3298–3309.
Liedberg, B., Nylander, C., Lundstrom, I., 1983. Sens. Actuators 4 (2), 299–304.
Malyarchuk, V., Hua, F., Mack, N.H., Velasquez, V.T., White, J.O., Nuzzo, R.G., Rogers, J.A., 2005. Opt. Expr. 13 (15), 5669–5675.
Miller, M.M., Lazarides, A.A., 2005. J. Phys. Chem. B 109 (46), 21556–21565.
Nagpal, P., Lindquist, N.C., Oh, S.-H., Norris, D.J., 2009. Science 325 (5940), 594–597.
Neuzil, P., Reboud, J., 2008. Anal. Chem. 80 (15), 6100–6103.
Stewart, M.E., Anderton, C.R., Thompson, L.B., Maria, J., Gray, S.K., Rogers, J.A., Nuzzo, R.G., 2008. Chem. Rev. 108 (2), 494–521.
Svedendahl, M., Chen, S., Dmitriev, A., Kall, M., 2009. Nano Lett. 9 (12), 4428–4433.